Enhanced angular characteristics of indium tin oxide nanowhisker-coated silicon solar cells

Chia-Hua Chang,[1] Min-Hsiang Hsu,[1] Ping-Chen Tseng,[1] Peichen Yu,[1,*] Wei-Lun Chang,[2] Wen-Ching Sun,[2] and Wei-Chih Hsu[2]

[1]*Department of Photonics and Institute of Electro-Optical Engineering, National Chiao-Tung University, 1001 Ta-Hsueh Road, Hsinchu, 300 Taiwan*

[2]*Green Energy & Environment Research Labs, Industrial Technology Research Institute, 195, Sec. 4, Chung Hsing Road, Chutung, Hsinchu, 310 Taiwan*

**yup@faculty.nctu.edu.tw*

Abstract: Omnidirectional and broadband light harvesting is critical to photovoltaics due to the sun's movement and its wide spectral range of radiation. In this work, we demonstrate distinctive indium-tin-oxide nanowhiskers that achieve superior angular and spectral characteristics for crystalline silicon solar cells using angle-resolved reflectance spectroscopy. The solar-spectrum weighted reflectance is well below 6% for incident angles of up to 70° and for the wavelength range between 400nm and 1000nm. As a result, the nanowhisker coated solar cell exhibits broadband quantum efficiency characteristics and enhanced short-circuit currents for large angles of incidence.

©2011 Optical Society of America

OCIS codes: (310.6628) Subwavelength structures, nanostructures; (040.5350) Photovoltaic.

References and links

1. B. S. Richards, "Comparison of TiO_2 and other dielectric coatings for buried contact solar cells: a review," Prog. Photovolt. Res. Appl. **12**(4), 253–281 (2004).
2. C. Martinet, V. Paillard, A. Gagnaire, and J. Joseph, "Deposition of SiO_2 and TiO_2 thin films by plasma enhanced chemical vapor deposition for antireflection coating," J. Non-Cryst. Solids **216**, 77–82 (1997).
3. V. M. Aroutiounian, K. Martirosyan, and P. Soukiassian, "Almost zero reflectance of a silicon oxynitride/porous silicon double layer antireflection coating for silicon photovoltaic cells," J. Phys. D Appl. Phys. **39**(8), 1623–1625 (2006).
4. P. B. Clapham and M. C. Hutley, "Reduction of lens reflection by the 'moth eye' principle," Nature **244**(5414), 281–282 (1973).
5. S. J. Wilson and M. C. Hutley, "The optical properties of 'moth eye' antireflection surfaces," Opt. Acta (Lond.) **29**, 993–1009 (1982).
6. P. Lalanne and G. M. Morris, "Antireflection behavior of silicon subwavelength periodic structures for visible light," Nanotechnology **8**(2), 53–56 (1997).
7. M. Srinivasarao, "Nano-optics in the biological world: beetles, butterflies, birds, and moths," Chem. Rev. **99**(7), 1935–1962 (1999).
8. M. Y. Chiu, C. H. Chang, M. A. Tsai, F. Y. Chang, and P. Yu, "Improved optical transmission and current matching of a triple-junction solar cell utilizing sub-wavelength structures," Opt. Express **18**(S3 Suppl 3), A308–A313 (2010).
9. Y. F. Huang, S. Chattopadhyay, Y. J. Jen, C. Y. Peng, T. A. Liu, Y. K. Hsu, C. L. Pan, H. C. Lo, C. H. Hsu, Y. H. Chang, C. S. Lee, K. H. Chen, and L. C. Chen, "Improved broadband and quasi-omnidirectional anti-reflection properties with biomimetic silicon nanostructures," Nat. Nanotechnol. **2**(12), 770–774 (2007).
10. Y. J. Lee, D. S. Ruby, D. W. Peters, B. B. McKenzie, and J. W. P. Hsu, "ZnO nanostructures as efficient antireflection layers in solar cells," Nano Lett. **8**(5), 1501–1505 (2008).
11. S. A. Boden and D. M. Bagnall, "Tunable reflection minima of nanostructured antireflective surfaces," Appl. Phys. Lett. **93**(13), 133108 (2008).
12. W. H. Southwell, "Gradient-index antireflection coatings," Opt. Lett. **8**(11), 584–586 (1983).
13. D. S. Hobbs, B. D. MacLeod, and J. R. Riccobono, "Update on the development of high performance anti reflecting surface relief micro-structures," Proc. SPIE **6545**, 65450Y, 65450Y-14 (2007).
14. C. H. Chang, P. Yu, and C. S. Yang, "Broadband and omnidirectional antireflection from conductive indium-tin-oxide nanocolumns prepared by glancing-angle deposition with nitrogen," Appl. Phys. Lett. **94**(5), 051114 (2009).
15. P. Yu, C. H. Chang, C. H. Chiu, C. S. Yang, J. C. Yu, H. C. Kuo, S. H. Hsu, and Y. C. Chang, "Efficiency enhancement of GaAs photovoltaics employing antireflective indium tin oxide nanocolumns," Adv. Mater. (Deerfield Beach Fla.) **21**(16), 1618–1621 (2009).

#140970 - $15.00 USD Received 12 Jan 2011; revised 11 Mar 2011; accepted 11 Mar 2011; published 18 Mar 2011

16. X. S. Peng, G. W. Meng, X. F. Wang, Y. W. Wang, J. Zhang, X. Liu, and L. D. Zhang, "Synthesis of oxygen-deficient indium-tin-oxide (ITO) nanofibers," Chem. Mater. **14**(11), 4490–4493 (2002).
17. Y. Q. Chen, J. Jiang, B. Wang, and J. G. Hou, "Synthesis of tin-doped indium oxide nanowires by self-catalytic VLS growth," J. Phys. D Appl. Phys. **37**(23), 3319–3322 (2004).
18. H. Yumoto, T. Sako, Y. Gotoh, K. Nishiyama, and T. Kaneko, "Growth mechanism of vapor-liquid-solid (VLS) grown indium tin oxide (ITO) whiskers along the substrate," J. Cryst. Growth **203**(1-2), 136–140 (1999).
19. S. Takaki, Y. Aoshima, and R. Satoh, "Growth mechanisms of indium tin oxide whiskers prepared by sputtering," Jpn. J. Appl. Phys. **46**(No. 6A), 3537–3544 (2007).
20. C. H. Chiu, P. Yu, C. H. Chang, C. S. Yang, M. H. Hsu, H. C. Kuo, and M. A. Tsai, "Oblique electron-beam evaporation of distinctive indium-tin-oxide nanorods for enhanced light extraction from InGaN/GaN light emitting diodes," Opt. Express **17**(23), 21250–21256 (2009).
21. ASTMG173–03, Standard tables for reference solar spectral irradiances, (ASTM International, West Conshohocken, Pennsylvania, 2005).
22. A. Parretta, A. Sarno, P. Tortora, H. Yakubu, P. Maddalena, J. Zhao, and A. Wang, "Angle-dependent reflectance measurements on photovoltaic materials and solar cells," Opt. Commun. **172**(1-6), 139–151 (1999).
23. M. D. Kelzenberg, S. W. Boettcher, J. A. Petykiewicz, D. B. Turner-Evans, M. C. Putnam, E. L. Warren, J. M. Spurgeon, R. M. Briggs, N. S. Lewis, and H. A. Atwater, "Enhanced absorption and carrier collection in Si wire arrays for photovoltaic applications," Nat. Mater. **9**(3), 239–244 (2010).
24. J. L. Balenzategui and F. Chenlo, "Measurement and analysis of angular response of bare and encapsulated silicon solar cells," Sol. Energy Mater. Sol. Cells **86**(1), 53–83 (2005).
25. H. Sai, H. Fujii, K. Arafune, Y. Ohshita, Y. Kanamori, H. Yugami, and M. Yamaguchi, "Wide-angle antireflection effect of subwavelength structures for solar cells," Jpn. J. Appl. Phys. **46**(No. 6A), 3333–3336 (2007).

1. Introduction

Anti-reflective coatings (ARCs) play a very important role in optoelectronic devices, particularly solar cells [1–3]. The conventional ARCs are realized in general with a stack of thin-film dielectric layers, which involves a detailed optical design and precise evaporation controls to tailor for the broad solar spectrum. Over the past decade, versatile sub-wavelength structures (SWSs), such as biomimetic moth-eye structures [4–8] and random nano-rods [9–11], have demonstrated broadband and omnidirectional antireflection characteristics. The superior performance of SWSs results from a gradually varying structural profile or air porosity which functions as a graded index (GRIN) buffer layer at the dielectric interface [12,13]. However, the elaborated fabrication processes involving either electron-beam (e-beam) lithography and/or dry etching are not suitable for large-area solar cells. The process-induced surface recombination defects further deteriorate the device performance, hindering the wide deployment of SWSs in photovoltaics. Consequently, SWSs fabricated by using bottom-up growth methods are rather favorable for actual device applications. In this paper, we demonstrate a single layer of indium-tin-oxide nanowhiskers deposited on a micro-textured silicon solar cell using electron-beam evaporation [14,15]. The nanowhisker-coated solar cell exhibits superior omnidirectional and broadband antireflective properties, compared to a conventional reference cell. As a result, the power conversion efficiency (PCE) of the cell with the nanowhisker ARC achieves 17.18%, compared to 16.08% of the control cell. The enhancement in the external quantum efficiency (EQE) characteristics well matches the reduction in reflectivities, which confirm the enhanced light transmission and nearly lossless photo-electric conversion facilitated by ITO nanowhiskers. Moreover, the angular characteristics of solar cells with such combined micro- and nano-scale surface textures had yet been investigated. An angle-resolved reflectance spectroscopy and an angular current-voltage system are established to correlate the angle-dependent antireflection characteristics to the short-circuit-current enhancement.

2. Experimental

The device fabrication followed standard Si solar cell process procedures, including saw-damage and surface-texture etch using a KOH solution, emitter diffusion with $POCl_3$, deposition of a 80-nm-thick SiN_x passivation layer, and the screen-printing process for the front and back contacts. Subsequently, the ITO nanowhiskers were deposited using an electron-beam evaporation system by introducing 1 sccm nitrogen. Nitrogen can dilute the oxygen concentration in the chamber, facilitating the growth of ITO nanowhiskers in an

#140970 - $15.00 USD Received 12 Jan 2011; revised 11 Mar 2011; accepted 11 Mar 2011; published 18 Mar 2011
(C) 2011 OSA

oxygen deficient ambient. The composition of the ITO target included 95 wt% In_2O_3 and 5 wt% SnO_2. During the deposition, the chamber pressure was controlled at 10^{-4} torr with a substrate temperature of 260°C. Next, the nanowhisker-coated solar cell and the reference cell were co-fired in a fast- firing belt furnace at a peak temperature of 800°C. Finally, the edge isolation was achieved using a 532-nm Nd:YAG laser. The cell area is 2.5x3.5 cm^2.

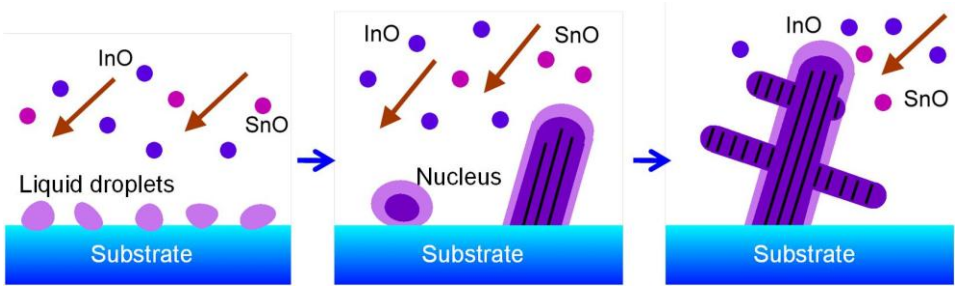

Fig. 1. The schematic formation of ITO nanowhiskers undergoing three steps: nucleation, column growth, and branch development. The growth mechanism is possibly dominated by a self-catalytic vapor-liquid-solid mechanism in an oxygen-deficient ambience.

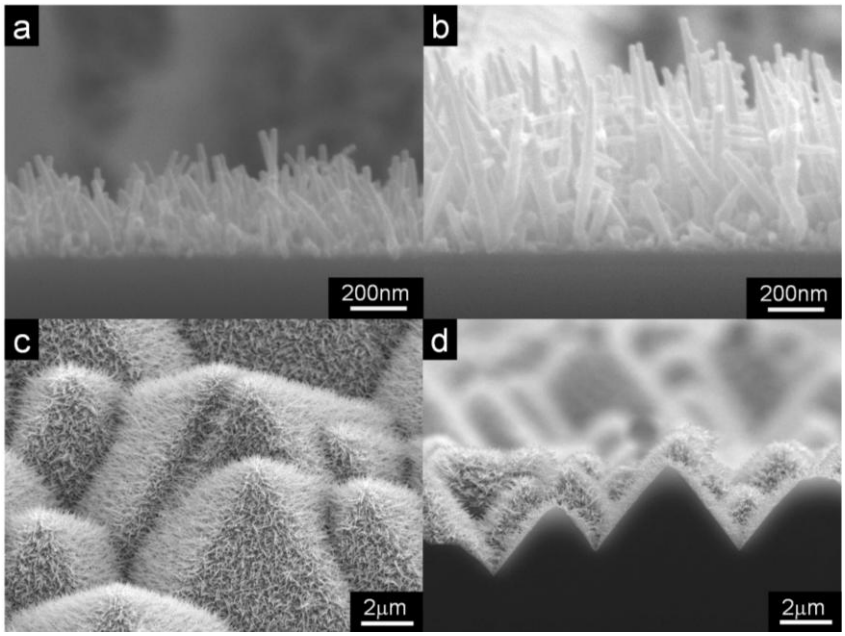

Fig. 2. Scanning electron micrographs (SEM) for ITO nanowhiskers deposited on micro-grooved silicon solar cells. (a) The initial step shows nanorod structure. (b) The optimized ITO nanowhisker structure. (c) The 45° tilted and (d) cross-sectional views of the optimized ITO nanowhiskers on microgrooves.

The growth of ITO nanowhiskers presumably involves a self-catalytic vapor-liquid-solid mechanism. Due to oxygen deficiency during the deposition, the tin atoms function as the catalyst in an In-Sn-O ternary phase, facilitating the development of a liquid phase on the surface [16,17]. As illustrated in Fig. 1, the growth of ITO nanowhiskers undergoes three steps. The first step is nucleation, where ITO molecules evaporated from the target form a thin film with a liquid phase on the surface due to oxygen deficiency. Then, the In_2O_3 molecules form crystalline nuclei inside the liquid shell and grow vertically into nanorods. At a height of ~700 nm, the In_2O_3 crystals no longer grow vertically but develop branches on the side by breaking through the Sn-rich liquid surface, forming into a whisker structure. An electron

#140970 - $15.00 USD Received 12 Jan 2011; revised 11 Mar 2011; accepted 11 Mar 2011; published 18 Mar 2011
(C) 2011 OSA

dispersive spectroscopic (EDS) analysis has been conducted and confirmed the surface of a trunk exhibiting a relatively high tin composition. Similar growth mechanisms have been reported by sputtering [18,19], and by oblique electron-beam evaporation [15,20]. Figures 2(a) to 2(d) show the scanning electron micrographs (SEMs) of the evaporated ITO nanowhiskers on the micro-grooves, where the whiskers are uniformly distributed. Figure 2(a) shows the scanning electron micrograph (SEM) at the column growth step, where short ITO rods exhibit a diameter of 30-50 nm and a height of 150-250 nm. Figure 2(b) shows the whisker structures with a longer deposition time, forming a much denser surface nanostructures than Fig. 2(a). The ITO nanowhiskers consist of one thick trunk and many short branches, where the branch density is related to the optical properties. At this point, Fig. 2(b) represents the best condition for the antireflection properties of the silicon solar cell, which is discussed next. The height of the trunk is approximately 750 nm and the diameter is approximately 50 nm. Figure 2(c) and 2(d) show 45° tilted and cross-sectional views of the optimized ITO nanowhiskers, respectively.

3. Results and discussion

The fabricated solar cells are characterized under a standard test condition with a simulated AM1.5g illumination (100mW/cm^2). The current-voltage characteristics are plotted in Fig. 3(a). The short-circuit current density (J_{sc}) of the solar cell with ITO nanowhiskers (the whisker cell) increased from 35.84 mA/cm^2 to 37.36 mA/cm^2, differed by an additional 1.52mA/cm^2. The PCE is also enhanced by 7% (from 16.08% to 17.18%) by using ITO nano-whiskers with a height of 750 nm as an ARC. Moreover, the external quantum efficiency (EQE) and reflectance at normal incident angles are measured for both the whisker and the reference cells. As shown in Fig. 3(b), the whisker cell demonstrates low reflectance (R<5%) for the wavelength range between 350 nm to 1100 nm, which increases the optical absorption of the solar cell in the near-infrared wavelength range. Consequently, the whisker cell demonstrates a higher EQE from 600 nm to 1100 nm than the reference due to improved optical absorption. ITO nanowhiskers effectively improve absorption in the near infrared, which is the usual weak absorption region for silicon photovoltaics. However, the ITO whiskers also exhibit parasitic absorption below 400 nm that slightly affected the EQE. It is worth noting that the internal quantum efficiency (IQE) spectra of both devices, obtained by dividing the measured EQE with R, are nearly identical for wavelengths larger than 400 nm, indicating that the improvement of EQE is purely due to reduced optical reflection. Moreover, based on the EQE measurement, the calculated photocurrent densities, obtained by integrating the product of the EQE and standard AM 1.5g spectrum over wavelength [21], are 38.76 mA/cm^2 and 37.48 mA/cm^2 for the whisker and the reference cells, respectively. The calculated values agree with the measurements within 4.5%, which also confirms the accuracy of the calibration and characterization procedures.

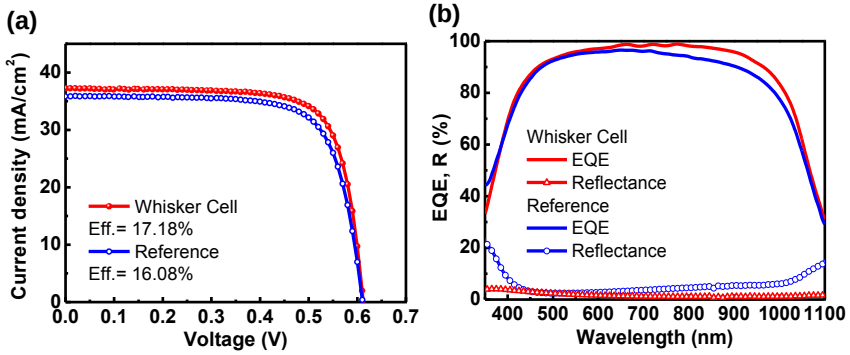

Fig. 3. (a) The current density-voltage curves of the solar cell with ITO nanowhiskers (the whisker cell) and the reference cell. (b) The external quantum efficiency (EQE) and reflectance (R) spectra at the normal incident angle for both whisker and reference cells.

#140970 - $15.00 USD Received 12 Jan 2011; revised 11 Mar 2011; accepted 11 Mar 2011; published 18 Mar 2011
(C) 2011 OSA

Figures 4(a) and 4(b) present an angle-resolved reflectance spectroscopy for both the reference and whisker cells, respectively [22,23]. It can be clearly seen that the reflection property at the near-infrared is detrimental for the reference cell, and further deteriorates with the increase in incident angles. As silicon photovoltaics are evolving towards thin substrate technologies, the high reflectivity at the near-infrared could further worsen the weak optical absorption in thin wafers. In contrast, the cell with ITO nanowhiskers suppresses optical reflection in the infrared wavelengths, as represented by the dark blue color on the right half plane of Fig. 4(b). Still, the surface textures may also give rise to scattering and slightly raise the reflectivity by less than 1% between the 500 and 600 nm wavelengths at oblique incident angles between 40° and 75°. However, it will also be shown later that the nearly negligible scattering loss does not affect the angular current-voltage characteristics.

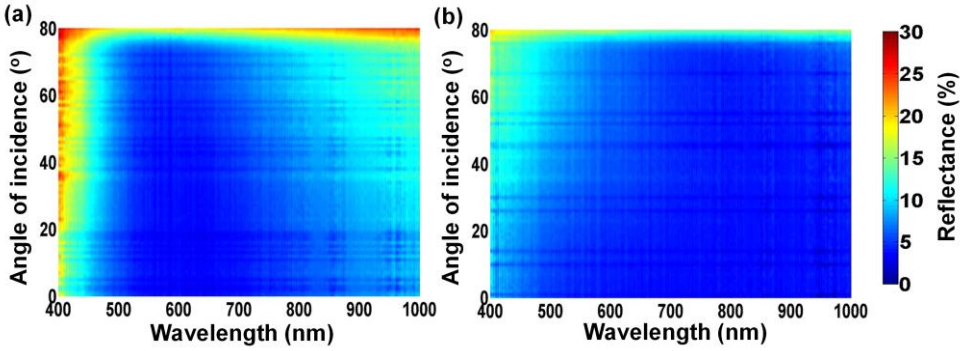

Fig. 4. Angle-resolved reflectance spectra for (a) reference cell and (b) ITO nanowhisker cell in the wavelength range of 400nm to 1000nm at the incident angle of 0 to 80 degree.

To quantitatively compare the angle-dependence of solar power harvesting, an AM 1.5g solar-spectrum weighted reflectance is further calculated using the following equation and plotted in Fig. 5(a).

$$< R(\theta) >= \frac{\int_{400nm}^{1000nm} R(\theta,\lambda) I_{AM1.5g}(\lambda) d\lambda}{\int_{400nm}^{1000nm} I_{AM1.5g}(\lambda) d\lambda}, \quad (1)$$

where R(θ,λ) is the measured reflectance maps shown in Fig. 4(a) and 4(b), and $I_{AM1.5g}$ (λ)is the photon flux density of the AM1.5g solar spectrum. As shown in Fig. 5(a), the weighted reflectance of the whisker cell shows a remarkable decrease compared to the control cell, particularly at large angles of incidence. At an incident angle of 70°, the weighted reflectance <R> of the whisker cell is still less than 7%, while that of reference cell is approximately 9%. The omnidirectional property is further investigated by mounting the cell on a homemade rotatable chuck and performing the I-V characterization under the AM 1.5g condition from zero to 85° [24,25]. The angular short-circuit current density for both cells and the corresponding enhancement factor are plotted in Fig. 5(b). The measured curves generally follow the cosine law due to the oblique incidence of light. As shown in Fig. 5(b), the enhanced short-circuit current density of the whisker cell is sustained for large angles of incidence, where the corresponding enhancement factor becomes considerable at large angles, e.g. >15% at an incident angle of 70°. Both measurements in Figs. 4 and 5 indicate that a solar cell with ITO nanowhiskers coated on the micro-grooved surface could further improve the solar energy conversion for the entire day.

#140970 - $15.00 USD Received 12 Jan 2011; revised 11 Mar 2011; accepted 11 Mar 2011; published 18 Mar 2011
(C) 2011 OSA

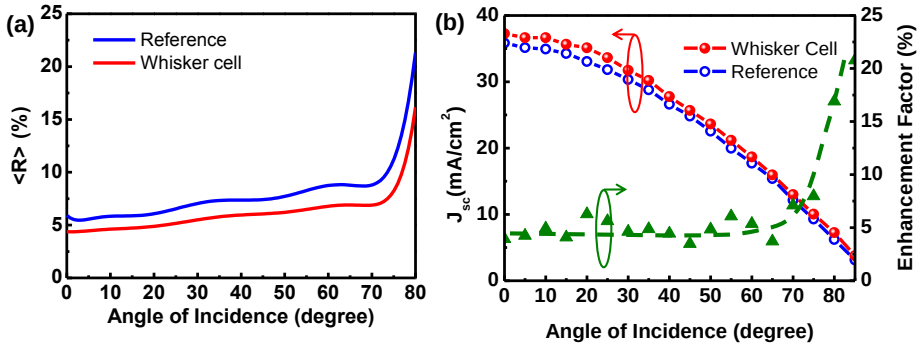

Fig. 5. (a)The weighted reflectance <R> of both cells, calculated by the AM1.5g solar spectrum intensity and the measured angular reflectance spectra shown in Fig. 4. (b) The angular photocurrent characterization of the nanowhisker cell (red) and the reference cell (blue). The green triangle shows the corresponding enhancement factor at different incident angles, where the dashed curve represents an eye guide.

4. Conclusion

In conclusion, we presented the enhanced angular characteristics of a silicon solar cell employing ITO nanowhiskers, which are grown by electron-beam deposition with a nitrogen flux. The uniform nanowhisker layer improves the external quantum efficiency in the near infrared wavelength range, and contribute to an increased short-circuit current and power conversion efficiency by an additional 1.52mA/cm^2 and 1.1%, respectively. An angle-resolved reflectance spectroscopy reveals the omnidirectional antireflective properties for the silicon solar cell coated with ITO nanowhiskers. The angular I-V characterization further confirms enhanced photocurrent conversion for large incident angles up to 85°.

Acknowledgment

The authors thank Prof. H. C. Kuo at National Chiao-Tung University for facility support. This work is supported by the National Science Council in Taiwan under grant number, NSC 96-2221-E-009-092-MY3, NSC 97-2120-M-006-009 and the Bureau of Energy and Ministry of Economic Affairs in Taiwan.

#140970 - $15.00 USD Received 12 Jan 2011; revised 11 Mar 2011; accepted 11 Mar 2011; published 18 Mar 2011
(C) 2011 OSA